



QUASI-STATIC LOADING PROTOCOLS FOR SDOF SYSTEMS UNDER LONG-PERIOD GROUND MOTIONS

B. Wang⁽¹⁾, Z. Li⁽²⁾, J. W. Zhang⁽³⁾, K. Yang⁽⁴⁾, T. Wu⁽⁵⁾, B. Q. Liu⁽⁶⁾

⁽¹⁾ Associate professor, School of Civil Engineering, Chang'an University, Xi'an, China, E-mail: chnwangbo@chd.edu.cn

⁽²⁾ Graduate student, School of Civil Engineering, Chang'an University, Xi'an, China, E-mail: li-zhechd@163.com

⁽³⁾ Graduate student, School of Civil Engineering, Chang'an University, Xi'an, China, E-mail: zaq197125zaq@163.com

⁽⁴⁾ Doctoral student, School of Civil Engineering, Chang'an University, Xi'an, China, E-mail: yangkechd@163.com

⁽⁵⁾ Professor, School of Civil Engineering, Chang'an University, Xi'an, China, E-mail: wutao@chd.edu.cn

⁽⁶⁾ Professor, School of Civil Engineering, Chang'an University, Xi'an, China, E-mail: bqliu@chd.edu.cn

Abstract

Due to abundant low-frequency components of long-period ground motions (LPGMs), long-period structures are susceptible to suffer severe damage, and the corresponding time-history displacement response curves of long-period structures under LPGMs have significant “large-displacement” and “long-duration” characteristics. These action characteristics essentially reflect the different loading paths of LPGMs from original ground motions (OGMs) imposed on structures. Hence, revealing the influence mechanism of this type of action characteristic on seismic performance of the structural component is the key to investigate the influence of LPGMs on the whole structure. The purpose of this study is to develop a kind of quasi-static loading protocol considering the action characteristics of LPGMs. Firstly, 50 representative LPGMs were selected to conduct nonlinear time-history analysis of single-degree-of-freedom (SDOF) systems. The inelastic cycles and corresponding displacement amplitudes of time-history displacement response curves under LPGMs were statistically analyzed through the rainflow counting algorithm. Then, influence factors of cycle number and displacement amplitude including the ground motion type, structural natural period, target ductility, strength reduction coefficient and damping ratio were discussed. Finally, the prediction model of cycle number and displacement amplitude was obtained by regression based on the structural natural period and target ductility. On this basis, the quasi-static loading protocol considering the action characteristics of LPGMs were developed. The proposed quasi-static loading protocol can be directly applied to the experimental investigations on the seismic performance of structural components which could be simplified as SDOF systems subjected to LPGMs.

Keywords: long-period ground motions, action characteristics, Single-degree-of-freedom, quasi-static loading protocols, rainflow counting algorithm



1 Introduction

Long-period ground motions (LPGMs) generally refer to the far-field ground motions with predominant periods of 1 s~10 s or longer, and the cause of LPGMs is mainly related to the propagation path of seismic waves [1]. Existing researches [2-4] indicated that the time-history displacement response curves of long-period structures under LPGMs have distinct characteristics of “large-displacement” and “long-duration”, which essentially reflects the different action paths of LPGMs from original ground motions (OGMs) imposed on structures. A plenty of researches showed that the loading path has a remarkable influence on the strength and stiffness deterioration, deformation performance, energy dissipation capacity and failure mechanism of structural components [5-16]. Therefore, it can be considered that revealing the influence mechanism of the LPGMs action characteristics, “large-displacement” and “long-duration”, on the seismic performance of structural components is the key to investigate the influence of LPGMs on the whole structure. The quasi-static test loading protocols considering the action characteristics of LPGMs could provide a possibility for the experimental investigation of the seismic performance and failure mechanism of structural components subjected to LPGMs. However, existing quasi-static loading protocols have not considered the LPGMs action characteristics, and there is no research concerning quasi-static loading protocols based on LPGMs.

The loading history of ground motions imposed on structures can be regarded as a random loading process. The load time-history can be converted into a series of full or half cycles through “counting algorithm”. Among the existing counting algorithms, rainflow counting algorithm is the most widely used counting algorithm, due to the consistency of counting procedure with stress-strain characteristics of materials, the better consideration of cycle distribution of random loading and reliable mechanical basis [17-18]. In recent years, some researches regarding quasi-static loading protocols considering the action characteristics of practical ground motions have been conducted based on the rainflow counting algorithm [19-28]. However, LPGMs were not taken into account in the existing researches, and the corresponding quasi-static loading protocols could not reflect the action characteristics of LPGMs.

Therefore, quasi-static loading protocols considering the action characteristics of LPGMs was proposed in this paper. RC pier columns in long-span bridges, which can be simplified as single-degree-of freedom (SDOF) system, were taken as the engineering background. Firstly, 50 representative LPGMs were selected to conduct nonlinear time-history analyses of SDOF systems, and the inelastic cycles and corresponding displacement amplitudes of time-history displacement response curves under LPGMs were statistically analyzed through the rainflow counting algorithm. Then, influence factors of cycle number and displacement amplitude including the ground motion type, structural natural period, target ductility, strength reduction coefficient and damping ratio were evaluated. Finally, the prediction model of displacement amplitude and cycle number considering the structural natural period and target ductility was proposed by regression. On this basis, the quasi-static loading protocols for SDOF systems under LPGMs were developed.

2 Nonlinear time-history analyses

50 representative LPGMs from Chi-Chi earthquake, WenChuan earthquake, East Japan earthquake and Tokachi earthquake were selected to conduct the nonlinear time-history analyses. 15 representative OGMs were also selected for the comparative analyses.

The RC pier column in long-span bridges were simplified as SDOF system. The Bouc-Wen-Baber-Noori (B-W-B-N) model [29-31], which considers strength and stiffness deterioration and the pinching effect comprehensively, was adopted to simulate the hysteretic behavior of structural components. Compared with other hysteresis models, it can better reflect the cumulative structural damage caused by LPGMs.

Inputting the selected ground motions into the simplified analysis model, the elastoplastic time-history displacement response could be obtained through the nonlinear time-history analyses. The target ductility of structural components was expected as the control index in the developed loading protocols. Therefore, the iterative amplitude modulation was conducted in time-history analyses, to ensure that the specific structural



components could reached the target ductility. Specifically, the peak ground acceleration (PGA) of each ground motion was increased from 0 with a constant increment of 0.1 gal, until the relative error between the calculated maximum ductility of the specific structural components (μ_{\max}) and the target ductility (μ) is less than or equal to 0.001. The calculation flow chart of nonlinear time-history analyses is shown in Fig. 1.

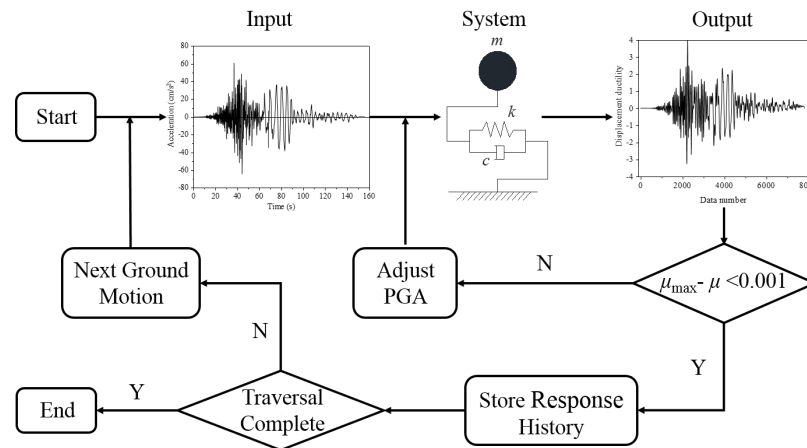


Fig. 1 The calculation flow chart of nonlinear time-history analyses

3 Rainflow cycle counting

3.1 Improved four-peak-valley rainflow counting algorithm

An improved four-peak-valley rainflow counting algorithm with higher counting efficiency was proposed in this paper. It could extract all cycles on the time-history displacement response curves using rainflow counting only once. The representative time-history displacement response curves of SDOF systems is shown in Fig. 2(a). The extraction steps are presented as follows.

(1) Convergence processing

The convergence processing is aimed to ensure the overall convergence of time-history displacement response curves. Reversing the two segments separated by the point with the maximum absolute value on the time-history displacement response curves and the convergence processing was accomplished. Fig. 2(b) presents the convergence processing result of the representative time-history displacement response curves.

(2) Peak-valley points extraction

The peak (valley) point is defined as the point whose displacement on the time-history displacement response curves is larger (less) than that of all two adjacent points. During the extraction, the peak-valley points were reserved, while the non-peak-valley points were discarded. The start and the ending points were directly reserved since they only have one adjacent point. The peak-valley points extraction result of the representative time-history displacement response curves is shown in Fig. 2(c).

(3) Cycle counting

After the convergence processing and the peak-valley points extraction, the time-history displacement response curves could be directly applied to the rainflow cycle counting. The judgment criterion of cycle counting is shown in Eqs. (1) and (2). A cycle could be counted when any of these criteria were satisfied, as shown in Fig. 2(d). And the corresponding displacement amplitudes could be calculated by Eq. (3). At the end of the cycle counting, only three points were left forming the last cycle. An example of cycle counting is shown as Fig. 2(e). The rainflow counting results of the representative time-history displacement response curves in ascending order of displacement amplitude is depicted in Fig. 2(f).

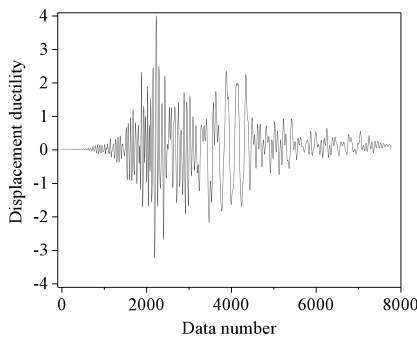
$$D_i \leq D_{i+2} \ \& \ D_{i+1} \leq D_{i+3}; \ i = 1, 2, \dots \quad (1)$$



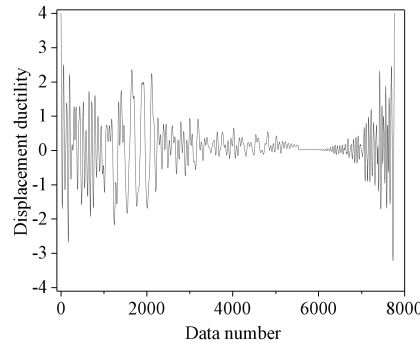
$$D_i \geq D_{i+2} \ \& \ D_{i+1} \geq D_{i+3}; \ i = 1, 2, \dots \quad (2)$$

$$D(n) = \frac{|D_{i+1} - D_{i+2}|}{2}; \ i = 1, 2, \dots \quad (3)$$

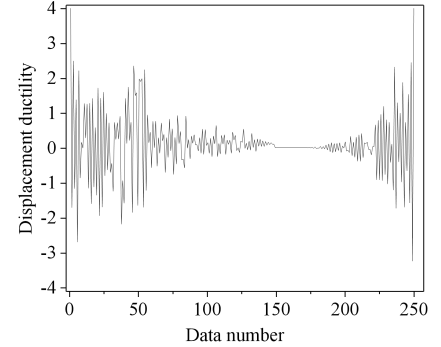
Where, D_i is the displacement of the i -th point; $D(n)$ is the displacement amplitude of the n -th cycle.



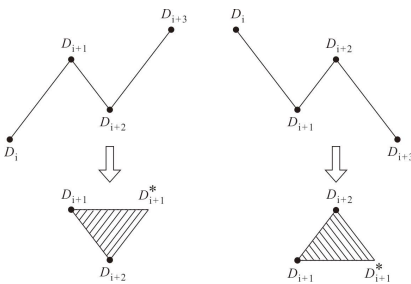
(a) Representative time-history displacement response curves



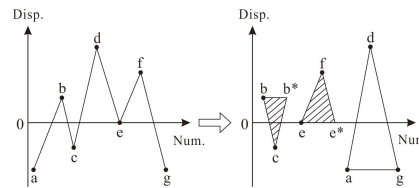
(b) Convergence processing results



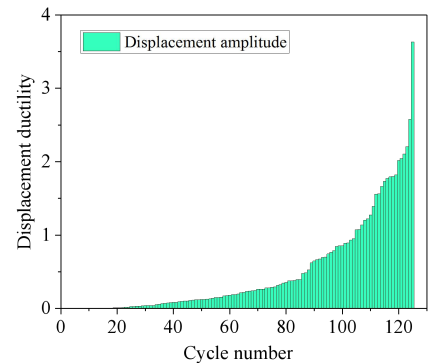
(c) Peak-valley points extraction results



(d) The judgment criterion of cycle counting



(e) An example of cycle counting



(f) Rainflow cycle counting results

Fig. 2 The counting process of four-peak-valley rainflow counting algorithm

3.2 Total inelastic cycle number N_{all} and maximum cumulative displacement ductility CDD_{max}

Every inelastic cycle contributes to the structural damage, and the damage degree depends on the inelastic cycle number and displacement amplitude distribution, which are two important indicators for loading protocols. However, these two indicators could not directly used for the comparison of loading protocols. Thus, the total inelastic cycle number N_{all} and the maximum cumulative displacement ductility CDD_{max} were introduced to quantitatively describe the inelastic cycle number and displacement amplitude distribution [20].

The total inelastic cycle number N_{all} is the sum of all numbers of inelastic cycles. The maximum cumulative displacement ductility CDD_{max} is the sum of the displacement amplitudes corresponding to all inelastic cycles. Two loading protocols with the same N_{all} may have different displacement amplitude distributions, those with the same CDD_{max} may have different inelastic cycle numbers and displacement amplitude distributions, reflecting the difference of loading protocols.

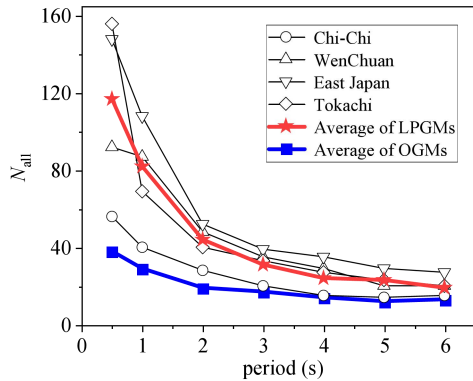
4 Influence factors of cycle number and displacement amplitude distribution

4.1 Ground motion type

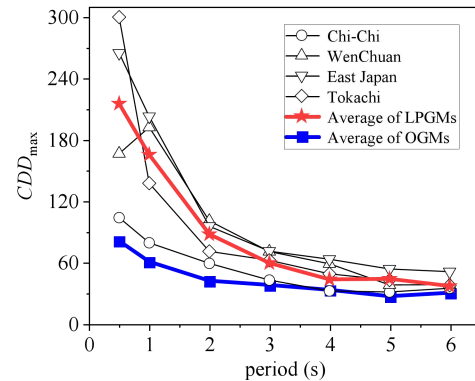


Fig. 3 presents the total inelastic cycle number N_{all} and the maximum cumulative displacement ductility CDD_{max} of SDOF systems with different periods under different types of ground motion. Where the target ductility factor is 4; the strength reduction coefficient is 4; the damping ratio is 0.05. All the data are the average values.

It can be observed that the ground motion type had a significant influence on the total inelastic cycle number N_{all} and the maximum cumulative displacement ductility CDD_{max} . The N_{all} and CDD_{max} under LPGMs were significantly larger than those under OGMs. This could be attributable to the “long-duration” action characteristics of LPGMs.



(a)The total inelastic cycle number

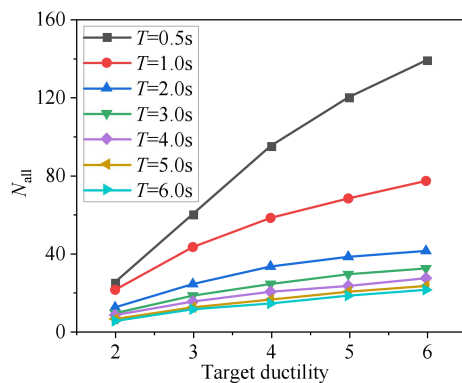


(b)The maximum cumulative displacement ductility

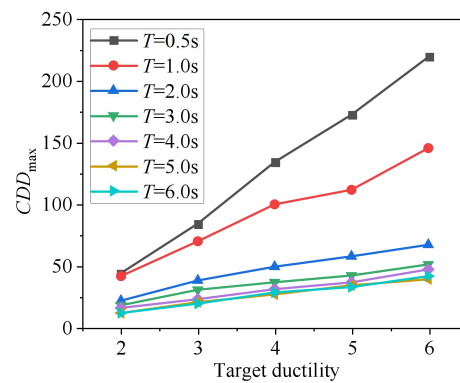
Fig. 3 The influence of ground motion type

4.2 Target ductility and structural natural period

Fig. 4 presents the total inelastic cycle number N_{all} and the maximum cumulative displacement ductility CDD_{max} of SDOF systems with different periods and target ductilities. Where the strength reduction coefficient is 4; the damping ratio is 0.05; T is the structural natural period.



(a)The total inelastic cycle number



(b)The maximum cumulative displacement ductility

Fig. 4 The influence of target ductility and structural natural period

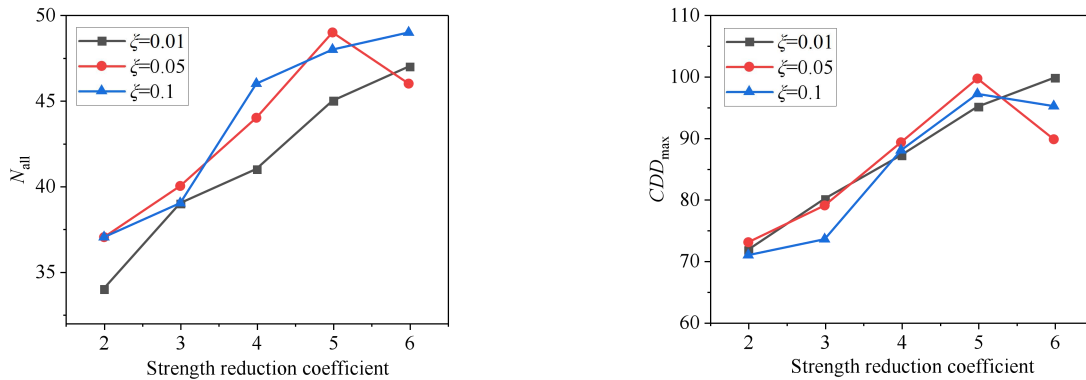
It can be observed that the target ductility and structural natural period had a remarkable influence on the total inelastic cycle number N_{all} and the maximum cumulative displacement ductility CDD_{max} . The N_{all} and CDD_{max} increased with the increase in target ductility. The N_{all} and CDD_{max} of SDOF systems with different periods presented consistent trends as the target ductility increased. And the CDD_{max} increased linearly as the target ductility increased, implying that with the increase in target ductility, the structures suffered more serious damage at the later loading stage with larger displacement amplitude. It also can be found that the N_{all} and CDD_{max} decreased with the increase in structural natural period. The reduction of N_{all}



and CDD_{max} was significant when the period was less than 2 s, while it slowed down when the period was in the range of 2 s~6 s.

4.3 Strength reduction coefficient and damping ratio

Fig. 5 presents the total inelastic cycle number N_{all} and the maximum cumulative displacement ductility CDD_{max} of SDOF systems with different strength reduction coefficients and damping ratios. Where the target ductility factor is 4; the structural natural period is 2 s; ζ is the damping ratio.



(a) The total inelastic cycle number

(b) The maximum cumulative displacement ductility

Fig. 5 The influence of strength reduction coefficient and damping ratio

It can be observed that, for SDOF systems with different damping ratios, N_{all} and CDD_{max} had the similar changing trends varying the strength reduction coefficient. While, for SDOF systems with the same damping ratio, increasing the strength reduction coefficient, N_{all} increased and CDD_{max} presented a linear increase except when the strength reduction coefficient was 6. While compared with Fig.4, the growth of N_{all} and CDD_{max} caused by the increase in strength reduction coefficient was less than that caused by the increase in target ductility and the decrease in structural natural period.

5 Double exponential regression prediction model

5.1 Double exponential regression prediction model

From the above analyses, it can be found that structural natural period and target ductility have the most significant influence on the cycle number and displacement amplitude distribution of loading protocols under a certain type of ground motion. Therefore, according to the regression statistical analysis results of cycle numbers and displacement amplitudes of SDOF systems with different periods and target ductilities, a double exponential regression prediction model of loading protocols considering the action characteristics of LPGMs was proposed, as shown in Eq. (4). The boundary conditions are $D(1)=1$ and $D(N_{all})=\mu$.

$$D(N) = \frac{1}{e^\alpha - e^\beta} [(\mu - e^\beta) e^{\alpha \frac{N-1}{N_{all}-1}} - (\mu - e^\alpha) e^{\beta \frac{N-1}{N_{all}-1}}] \quad (4)$$

Where, $D(N)$ is the displacement amplitude corresponding to the N -th cycle; N is the cycle number, valued as 1, 2, 3... N_{all} in turn; α and β are the distribution parameters of displacement amplitude, which reflect the trend of displacement amplitude $D(N)$ with the change of cycle number N ; μ is the target ductility factor.

5.1.1 The total inelastic cycle number N_{all}

The fitting formula of the total inelastic cycle number, taking target ductility factor and structural natural period as the independent variables, is shown in Eq. (5).

$$N_{all}(T, \mu) = C_s \cdot (L_T \times R_\mu) \quad (5)$$



Where, C_S is the coefficient matrix applied for SDOF system; L_T is the column vector associated with the structural natural period T ; R_μ is the row vector associated with the target ductility factor μ ; symbol $\cdot \times$ is the dot product operation of the matrix.

$$C_S = \begin{bmatrix} -16.62 & -15.75 & 34.16 & -6.352 & 0.3829 \\ 43.47 & -32.81 & -10.94 & 1.914 & -0.1053 \\ -9.783 & 24.55 & 0.1291 & -0.02959 & 0 \\ -5.83 & -4.574 & 0.01212 & 0 & 0 \\ 1.982 & 0.2954 & 0 & 0 & 0 \\ -0.162 & 0 & 0 & 0 & 0 \end{bmatrix} \quad (6)$$

$$L_T = [1 \quad T \quad T^2 \quad T^3 \quad T^4 \quad T^5]^T \quad (7)$$

$$R_\mu = [1 \quad \mu \quad \mu^2 \quad \mu^3 \quad \mu^4] \quad (8)$$

5.1.2 The distribution parameters of displacement amplitude α and β

The cumulative displacement amplitude distribution index CDF [20] was introduced to describe the trend of displacement amplitude distribution with the change of cycle number, which can be derived by Eq. (9). Fig. 6 presents the CDF of SDOF systems with different periods and target ductilities.

$$CDF = \frac{\sum N_i}{N_{all}} \quad (9)$$

Where, $\sum N_i$ is the number sum of cycles whose displacement amplitude is less than or equal to the displacement amplitude corresponding to the i -th cycle.

It can be observed in Figs. 6(a) and 6(b) that, with the same target ductility, the CDF of SDOF systems with different periods were almost the same, and they exhibited a greater agreement with each other as the target ductility increased. However, the CDF of SDOF systems with the same period showed a high dependence on the target ductility, as shown in Fig. 6(c). For the same value of CDF , the larger the target ductility, the larger the corresponding displacement amplitude was. Meanwhile, for SDOF systems with the same period, as the target ductility increased, the growth rate of displacement amplitude increased, while the difference of displacement amplitudes under two adjacent target ductility levels decreased.

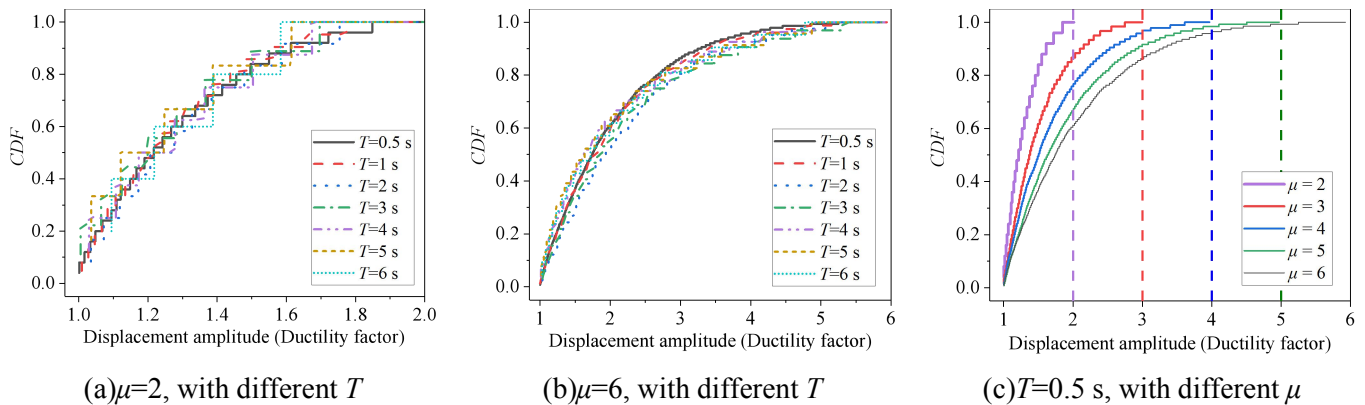


Fig. 6 The CDF of SDOF systems with different periods and target ductilities

Accordingly, for SDOF systems with the same target ductility, the regression prediction model with the same α and β should be adopted. The values of α and β should be the optimal fitting results of Eq. (4) according to the statistical cycle numbers and displacement amplitudes. The calculated optimal fitting parameters α and β for SDOF systems with different target ductilities are listed in Table 1.



Moreover, there was a small difference between the displacement amplitudes of SDOF systems with two high adjacent target ductility levels, and the growth rate of the displacement amplitude of SDOF systems with higher-level target ductility was larger compared with that with lower-level target ductility. Therefore, when the ductility factor of the practical structures is a non-integer, the cycle numbers and displacement amplitudes could be predicted by the parameter α and β under the closest integer high-level target ductility, as a conservative estimation value.

Table 1 Calculated distribution parameters of displacement amplitude α and β

Parameter	Target ductility factor μ				
	2	3	4	5	6
α	7.495	12.16	15.78	20.88	25.96
β	0.4199	0.6847	0.8765	1.068	1.207

5.1.3 The prediction of cycle numbers and displacement amplitudes

The cycle numbers and displacement amplitudes of loading protocols considering the action characteristics of LPGMs could be directly predicted by the proposed double exponential regression prediction model, instead of conducting the nonlinear time-history analyses. The specific steps of prediction are shown as follows.

Firstly, calculating the total inelastic cycle number N_{all} by Eq. (5) according to the structural natural period and target ductility. Then, in terms of the target ductility, obtaining the distribution parameters of displacement amplitude α and β from Table 1. Finally, the corresponding displacement amplitudes of all cycles could be calculated inputting the total inelastic cycle number N_{all} and distribution parameters α , β to Eq. (5).

5.2 Validation of proposed double exponential regression prediction model

In order to validate the accuracy and reliability of proposed regression prediction model, three RC bridge pier columns were designed based on displacement design method, representing SDOF system. The top mass of all three columns was 500 t, the height was 5 m, 10 m and 15 m respectively. The uniaxial compressive strength of the concrete was 40 MPa. The elastic modulus of reinforced concrete was 31.62 GPa. The damping ratio was set as 0.05, the target ductility factor was set as 4, and the structural natural period was 1.14 s, 2.26 s and 2.77 s, respectively. The equivalent stiffness of the columns was 15188.7 kN/m, 3864.7 kN/m and 2572.6 kN/m, respectively.

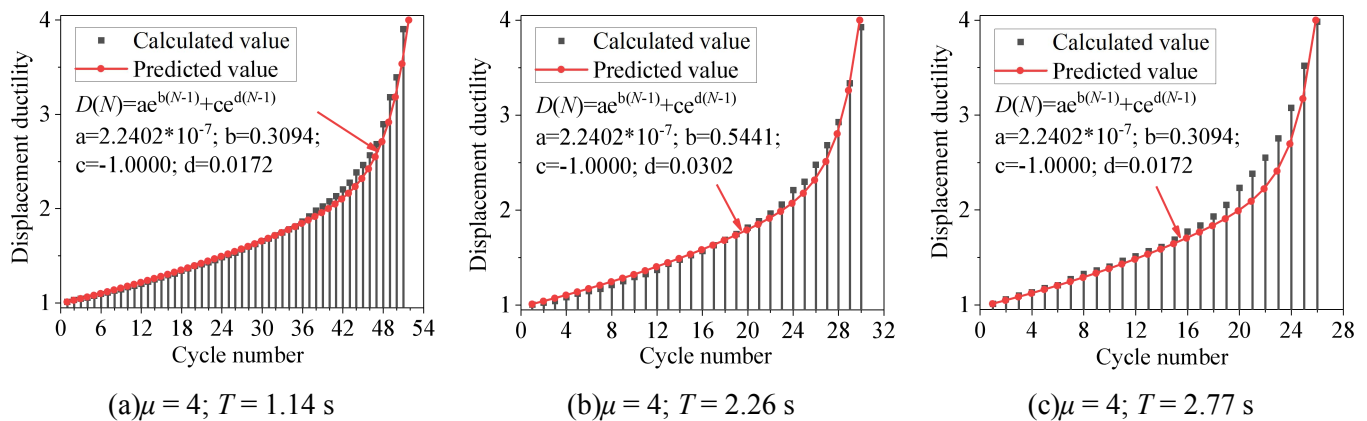


Fig. 7 Validation of the cycle number and displacement amplitude

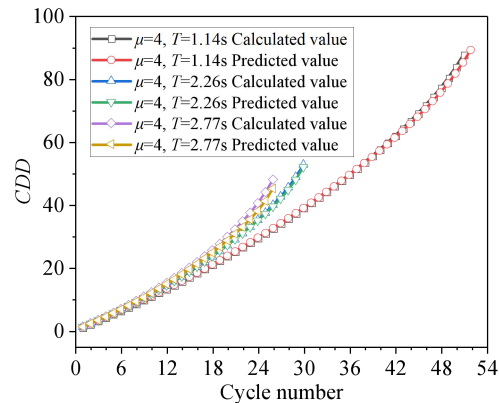


Fig. 8 Validation of the cumulative displacement ductility

The nonlinear time-history analyses and rainflow cycle counting were carried out first, obtaining the calculated actual cycle numbers and displacement amplitudes. Then, the predicted values of cycle numbers and displacement amplitudes were obtained by the proposed regression prediction model. Figs. 7 and 8 present the comparison of calculated and predicted values in cycle number, displacement amplitude and cumulative displacement ductility.

It can be observed in Fig. 7 that the predicted values of cycle number were in a good agreement with the calculated values. The predicted values of displacement amplitude basically coincided with the calculated values in the earlier stage, while those were slightly different from the calculated values in the later stage. This difference had a relatively small impact on the whole prediction model due to the large displacement amplitude in the later stage.

It can be seen in Fig. 8 that the predicted and calculated values of the cumulative displacement ductility were almost the same. This implied that, from the perspective of cumulative damage, the difference of displacement amplitude values in the later stage had almost no influence, which further validated the accuracy and reliability of the proposed double exponential regression prediction model.

6 Developed quasi-static loading protocols

Based on the proposed double exponential regression prediction model, the quasi-static loading protocols considering the action characteristics of LPGMs were developed. The protocols consisted of two stages: force-control loading stage and displacement-control loading stage. The RC pier column with target ductility factor of 4 and natural period of 2.26 s was taken as the example, the developed quasi-static loading protocol is shown in Fig. 9.

(1) The first loading stage (force-control loading stage)

When the displacement amplitude was less than the yield displacement δ_y , that is before the yielding of structural components, there was almost no damage. Hence, the loading protocols in different cases could adopt the same loading method in this stage. Force-control loading was employed in this paper. There were two cycles, as shown in Fig. 9. The first cycle was applied with the amplitude of $0.75 F_y$ (F_y is the theoretical yield load of structural components), and the second cycle was applied with the amplitude of F_y . The yielding of the column depends on the tension strain of longitudinal rebars on the control section. The lateral displacement of the horizontal actuator could be regard as the yield displacement (δ_y) when the tension strain of longitudinal rebars on the control section reached the yield strain.

(2) The second loading stage (displacement-control loading stage)

This stage aimed to reflect the influence of LPGMs action characteristics on structural components, which is the critical part for developed loading protocols. The cycle numbers and displacement amplitudes in this stage were predicted by the proposed prediction model, as shown in Fig. 7(b).



In order to regularize the loading protocols, it is necessary to grade the predicted displacement amplitude and recount the corresponding cycle number based on the predicted results. The target displacement amplitude, i.e. the target ductility factor (μ) multiplied the yield displacement (δ_y), was divided to 10 grades with an approximately equal interval, and the cycle numbers corresponding to the graded displacement amplitudes were recounted based on the predicted results. The graded displacement amplitudes and corresponding cycle numbers of representative RC column are shown in Table 2.

Table 2 The graded displacement amplitudes and corresponding cycle numbers

Grade	①	②	③	④	⑤	⑥	⑦	⑧	⑨	⑩
Graded displacement amplitude ($\times\delta_y$)	1	1.3	1.6	1.9	2.2	2.5	2.8	3.1	3.4	4
Cycle number	5	8	6	4	3	1	1	0	1	1

As shown in Table 2, it can be found that in the second loading stage, the RC column may be at the state of long-term damage accumulation instead of failure. In this case, the conventional quasi-static loading protocols with monotone increase of displacement amplitude should be applied after the second loading stage until the failure occurred. Thereby, the damage accumulation and residual bearing capacity of structural components considering the action characteristics of LPGMs could be comprehensively analyzed through the quasi-static tests.

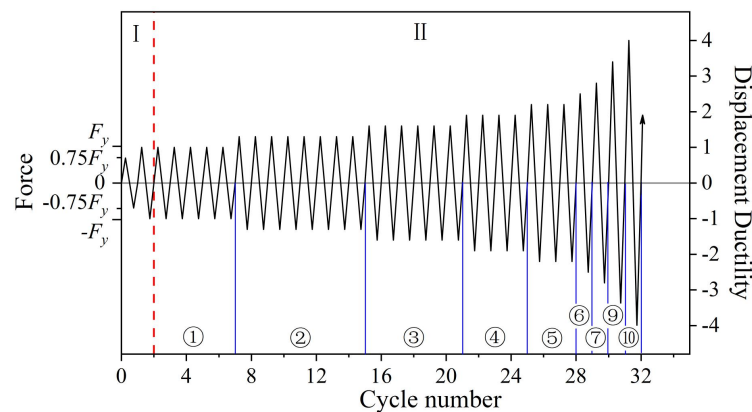


Fig. 9 Developed quasi-static loading protocols for SDOF system under LPGMs

7 Conclusions

The quasi-static loading protocols considering the action characteristics of LPGMs for the structural components which could be simplified as SDOF systems were developed in this paper. These protocols were developed by the regression prediction of the statistical time-history displacement response data under LPGMs. Results of time-history analyses were rainflow counted and statistical analyzed, and the prediction model of displacement amplitude and cycle number considering the influence of structural natural period and target ductility was proposed by regression. The predicted results were in accordance with the statistical data. The developed quasi-static loading protocols can be directly applied to the experimental study on the seismic performance of SDOF systems under LPGMs. While for the structural component that can not be simplified as SDOF system, it needs to be further studied.

Acknowledgements

This work is funded by the National Natural Science Foundation of China (NSFC, Grant No. 51708037 and 51978076), the support of which is gratefully acknowledged.



References

- [1] Koketsu K, Miyake H (2008): A seismological overview of long-period ground motion. *Journal of Seismology*, **12**(2), 133-143.
- [2] Chung YL, Nagae T, Hitaka T, Nakashima M (2010): Seismic resistance capacity of high-rise buildings subjected to long-period ground motions: E-Defense shaking table test. *Journal of Structural Engineering*, **136**(6), 637-644.
- [3] Takewaki I, Murakami S, Fujita K, Yoshitomi S, Tsuji M (2011): The 2011 off the pacific coast of Tohoku earthquake and response of high-rise buildings under long-period ground motions. *Soil Dynamics and Earthquake Engineering*, **31**(11), 1511-1528.
- [4] Wang B (2013): Study on dynamic behavior and design method of high-rise structures under multi-type long period ground motions. Xi'an University of Architecture and Technology, Xi'an. (in Chinese)
- [5] Kawashima K, Koyama T (1988): Effect of number of loading cycles on dynamic characteristics of reinforced concrete bridge pier columns. *Structural Engineering/Earthquake Engineering*, **5**(1), 205-213.
- [6] Pujol S, Sozen MA, Ramirez JA (2006): Displacement history effects on drift capacity of reinforced concrete columns. *ACI Structural Journal*, **103**(2), 253-262.
- [7] Acun B, Sucuoglu H (2010): The effect of displacement history on the performance of concrete columns in flexure. *Advances in Performance-Based Earthquake Engineering*, **13**, 373-382.
- [8] Goodnight JC, Kowalsky MJ, Nau JM (2013): Effect of load history on performance limit states of circular bridge columns. *Journal of Bridge Engineering*, **18**(12), 1383-1396.
- [9] Goodnight JC, Kowalsky MJ, Nau JM (2016): Strain limit states for circular RC bridge columns. *Earthquake Spectra*, **32**(3), 1627-1652.
- [10] Goodnight JC, Kowalsky MJ, Nau JM (2016): Modified plastic-hinge method for circular RC bridge columns. *Journal of Structural Engineering*, **142**(11), 04016103.
- [11] Feng YH, Kowalsky MJ, Nau JM (2015): Effect of seismic load history on deformation limit states for longitudinal bar buckling in RC circular columns. *Journal of Structural Engineering*, **141**(8), 04014187 (1-13).
- [12] Kowalsky MJ (2000): Deformation limit states for circular reinforced concrete bridge columns. *Journal of Structural Engineering*, **126**(8), 869-878.
- [13] Cook JNE, Gerstle KH (1985): Load history effects on structural members. *Journal of Structural Engineering*, **111**(3), 628-640
- [14] Lukunaprasit P, Thepmangkorn J (2004): Load History Effect on Cyclic Behavior of Reinforced Concrete Tied Columns. *Journal of Structural Engineering*, **130**(10), 1629-1633.
- [15] Ergun S, Demir A (2014): Effect of Hysteretic Models on Seismic Behavior of Existing RC Structures. *Journal of Performance of Constructed Facilities*, **29**(6), 04014160.
- [16] Syntzirma DV, Pantazopoulou SJ, Aschheim M (2010): Load-history effects on deformation capacity of flexural members limited by bar buckling. *Journal of structural engineering*, **136**(1), 1-11.
- [17] Dowling SD, Socie DF (1982): Simple rainflow counting algorithms. *International Journal of Fatigue*, **4**(1), 31-40.
- [18] American Society for Testing and Materials (ASTM) (2011): Standard Practices for Cycle-Counting in Fatigue Analysis. *ASTM Standard E1049-85*, ASTM International, West Conshohocken, PA, USA.
- [19] Ou YC, Song JW, Wang PH, Adidharma L, Chang KC, Lee GC (2014): Ground motion duration effects on hysteretic behavior of reinforced concrete bridge columns. *Journal of Structural Engineering*, **140**(3), 36-49.
- [20] Bazaez R, Dusicka P (2016): Cyclic loading for RC bridge columns considering subduction megathrust earthquake. *Journal of Bridge Engineering*, **21**(5), 04016009 (1-13).
- [21] Shafei B, Zareian F (2008): Development of a quasi-static loading protocol for displacement-sensitive nonstructural building components. *14th World Conference on Earthquake Engineering WCEE*, Beijing, China.
- [22] Krawinkler H, Parisi F, Ibarra L, Ayoub A, Medina R (2001): Development of a testing Protocol for Woodframe Structures. *Report W-02*, CUREE-Caltech Woodframe Project, Stanford University, Stanford, California, USA.



- [23] Richards PW, Uang C (2006): Testing Protocol for Short Links in Eccentrically Braced Frames. *ASCE Journal of Structural Engineering*, **132**(8), 1183-1191.
- [24] Federal Emergency Management Agency (FEMA) (2007): Interim Testing Protocols for Determining the Seismic Performance Characteristics of Structural and Nonstructural Components. *FEMA 461*, Federal Emergency Management Agency, Washington, DC, USA.
- [25] Retamales R, Mosqueda G, Filiatrault A, Reinhorn AM (2011): Testing Protocol for Experimental Seismic Qualification of Distributed Nonstructural Systems. *Earthquake Spectra*, **27**(3), 835-856.
- [26] Hutchinson TC, Zhang J, Charles E (2011): Development of a drift protocol for seismic performance evaluation considering a damage index concept. *Earthquake Spectra*, **27**(4), 1049-1076.
- [27] Hutchinson TC, Wood RL (2013): Cyclic Load Protocol for Anchored Nonstructural Components and Systems. *Earthquake Spectra*, **29**(3), 817-842.
- [28] Mergos P, Beyer K (2014): Loading protocols for European regions of low to moderate seismicity. *Bulletin of earthquake Engineering*, **12**(6), 2507-2530.
- [29] Goda K, Hong HP, Lee CS (2009): Probabilistic characteristics of seismic ductility demand of SDOF systems with Bouc-Wen hysteretic behavior. *Journal of Earthquake Engineering*, **13**(5), 600-622.
- [30] Sengupta P, Li B (2013): Modified Bouc-Wen model for hysteresis behavior of RC beam-column joints with limited transverse reinforcement. *Engineering Structures*, **46**, 392-406.
- [31] Sengupta P, Li B (2017): Hysteresis Modeling of Reinforced Concrete Structures: State of the Art. *ACI Structural Journal*, **114**(1), 25-38.